Title

Structural mechanism of Myb—MuvB assembly

Journal

Proceedings of the National Academy of Sciences of the United States of America, 115(40)

ISSN

0027-8424

Authors

Guiley, Keelan Z

Iness, Audra N

Saini, Siddharth

et al.

Publication Date

2018-10-02

DOI

10.1073/pnas.1808136115

Peer reviewed

Structural mechanism of Myb–MuvB assembly

Keelan Z. Guiley[a], Audra N. Iness[b], Siddharth Saini[b], Sarvind Tripathi[a], Joseph S. Lipsick[c,d,e], Larisa Litovchick[b,1], and Seth M. Rubin[a,1]

[a]Department of Chemistry and Biochemistry, University of California, Santa Cruz, CA 95064; [b]Division of Hematology, Oncology and Palliative Care and Massey Cancer Center, Virginia Commonwealth University, Richmond, VA 23298; [c]Department of Pathology, Stanford University, Stanford, CA 94305-5324; [d]Department of Genetics, Stanford University, Stanford, CA 94305-5324; and [e]Department of Biology, Stanford University, Stanford, CA 94305-5324

Edited by Michael R. Botchan, University of California, Berkeley, CA, and approved August 20, 2018 (received for review May 10, 2018)

The MuvB transcriptional regulatory complex, which controls cell-cycle-dependent gene expression, cooperates with B-Myb to activate genes required for the G2 and M phases of the cell cycle. We have identified the domain in B-Myb that is essential for the assembly of the Myb–MuvB (MMB) complex. We determined a crystal structure that reveals how this B-Myb domain binds MuvB through the adaptor protein LIN52 and the scaffold protein LIN9. The structure and biochemical analysis provide an understanding of how oncogenic B-Myb is recruited to regulate genes required for cell-cycle progression, and the MMB interface presents a potential therapeutic target to inhibit cancer cell proliferation.

cell cycle | transcription factor | Myb | MuvB | DREAM

There are three paralogous *MYB* genes in vertebrates that code for transcription factors: *MYB* (c-Myb), *MYBL1* (A-Myb), and *MYBL2* (B-Myb). *MYB* and *MYBL1* are involved in recurrent chromosomal translocations in human leukemia, adenoid cystic carcinoma, and pediatric glioma (1–3). Increased levels of *MYBL2* expression have been observed in breast cancer and are a predictor of poor prognosis (4). Consistent with an essential role in proliferation, B-Myb is present in all mitotically cycling cells (5), and *MYBL2* germline knockout mice display an early embryonic lethal phenotype (6). In contrast, c-Myb and A-Myb appear to be tissue- and cell type-specific (7, 8).

The Myb protein architecture contains a DNA-binding domain, a transactivation domain, and a negative regulatory domain (NRD; Fig. 1*A*). The C terminus has been referred to as the NRD because deletion of this region in all three Myb proteins promotes the activation of Myb-regulated genes in cell-based reporter assays (9–12). In human leukemia, adenoid cystic carcinoma, and pediatric glioma, chromosomal rearrangements create fusion proteins with truncations of the C terminus of c-Myb or A-Myb that remove the NRD and result in increased Myb target gene expression (1–3). The NRD is also absent in the transforming avian retroviral oncogene *V-MYB*, and deletion of the C terminus of c-Myb, in a fashion similar to v-Myb, is sufficient for oncogenic activation (3, 10).

Other evidence suggests that the C terminus of B-Myb primarily plays an activating role. Unlike the other family members, C-terminal truncation of the *MYBL2* gene in human cancers has not been reported. The C terminus of human B-Myb has been observed to enhance transcriptional activation when fused to c-Myb (13). Moreover, the C terminus of *Drosophila* Myb (dMyb), an ortholog of B-Myb, is essential for association with the MuvB complex, and mutations in this region abolish its activity (14, 15). These results suggest that part of the NRD may have some activating function related to Myb–MuvB (MMB) complex assembly, but further structure-function analysis of this domain is needed.

The MuvB complex cooperates with B-Myb during S-phase of the cell cycle to activate mitotic genes (16, 17). Cells require the MuvB complex and B-Myb or dMyb to undergo mitosis, as disruption of the MMB complex results in abnormal spindle assembly (14, 15, 17, 18). Essential G2/M cell-cycle genes activated by MMB contain a cell-cycle homology region (CHR) DNA element in their promoters (16, 17, 19, 20). The MuvB complex is assembled from five core proteins: RBAP48, LIN54, LIN52, LIN37, and LIN9 (16, 21–24). This MuvB core binds the retinoblastoma protein paralog p130 and the transcription factors E2F4/5-DP1/2 to form the DREAM complex, which represses cell-cycle genes in quiescence and in G1 phase (16, 23, 24). In S phase, MuvB dissociates from p130 and B-Myb binds to form MMB (17, 20, 25). RBAP48 is a histone-binding protein, and LIN54 directly binds the CHR DNA element in cell-cycle gene promoters (26, 27). LIN52 mediates MuvB association with p130 to form DREAM (25, 28). LIN9 and LIN37 have poorly characterized biochemical functions, but are required for MuvB-regulated gene expression (18, 29).

These studies suggest that B-Myb function is linked to the MuvB complex and the CHR element, from which it can activate genes required for mitosis. Here we present the structure of the C terminus of B-Myb and define its role as a MuvB-binding domain (MBD). We find that B-Myb assembles with the MuvB complex by accessing domains of LIN52 and LIN9. Our findings describe a conserved role for this MMB interface in cell-cycle progression and highlight a unique target for cancer therapeutics.

Results

Determinants for Assembly of the MMB Complex. We first identified the B-Myb domain requirements for human MMB complex assembly. Using a coimmunoprecipitation assay in T98G cells, we

Significance

Myb family transcription factors are potent activators of cell proliferation and drivers of human cancer. B-Myb, the most ancient and conserved family member, induces transcription of mitotic genes. The MuvB complex, thought to be the master regulator of cell-cycle-dependent gene expression, is required for directing B-Myb to the proper promoters. We present a structural description of MuvB and how it recruits B-Myb. We identified a direct association between the B-Myb C-terminus and the MuvB components LIN9 and LIN52, and we determined the crystal structure of this subcomplex. Our data define LIN52 as a central transcription factor-binding hub in MuvB and reveal a Myb–MuvB interface that could be targeted with chemical inhibitors.

Author contributions: K.Z.G., J.S.L., L.L., and S.M.R. designed research; K.Z.G., A.N.I., S.S., and S.T. performed research; K.Z.G., A.N.I., S.S., S.T., L.L., and S.M.R. analyzed data; and K.Z.G., J.S.L., L.L., and S.M.R. wrote the paper.

The authors declare no conflict of interest.

This article is a PNAS Direct Submission.

Data deposition: The atomic coordinates and structure factors have been deposited in the Protein Data Bank, www.wwpdb.org (PDB ID code 6C48).

[1]To whom correspondence may be addressed. Email: larisa.litovchick@vcuhealth.org or srubin@ucsc.edu.

This article contains supporting information online at www.pnas.org/lookup/suppl/doi:10.1073/pnas.1808136115/-/DCSupplemental.

Published online September 17, 2018.

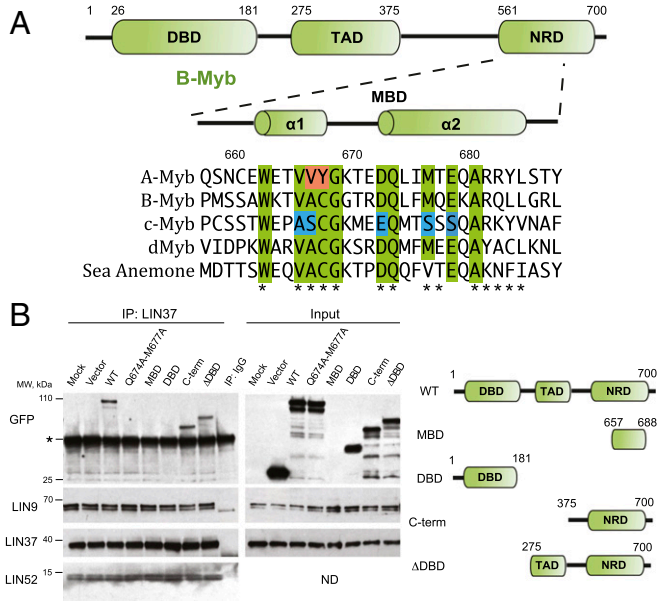

Fig. 1. The B-Myb C-terminal domain is necessary and sufficient for MuvB association. (*A*) Domain architecture of Myb proteins (sequence numbering for human B-Myb), including a DNA-binding domain (DBD), transactivation domain (TAD), and a negative regulatory domain (NRD). The MuvB binding domain (MBD, residues 657–688) investigated here is within the NRD and has the aligned sequence. The secondary structure and amino acids that interact with MuvB (asterisks) are determined from the crystal structure in this study. Amino acids that are highly conserved in vertebrate B-Myb orthologs and *Drosophila* Myb (dMyb) are highlighted green, with changes at these positions in A-Myb and c-Myb shown in red and blue (*SI Appendix*, Fig. S1). (*B*) T98G cells were transfected with plasmids encoding the indicated GFP-B-Myb fusion protein. Vector expresses GFP only. Lysates were immunoprecipitated with an anti-LIN37 antibody, and Western blots performed to assay the protein of interest. The asterisk marks Ig bands from the primary antibody.

found that the C terminus of B-Myb (residues 375–700) is necessary and sufficient for association with LIN37 and other MuvB components (Fig. 1*B*), which was similarly observed in *Drosophila* dMyb (14). Mutating the conserved residues Q674 and M677 was sufficient to disrupt MMB complex formation. On the basis of these data, the sequence conservation in the Myb C terminus (Fig. 1*A* and *SI Appendix*, Fig. S1), and our previous observation that B-Myb residues 654–700 are sufficient to bind recombinant MuvB (25), we conclude that the C terminus of B-Myb contains a MBD. A small fragment of the B-Myb C terminus (Fig. 1*B*, residues 657–688, hereafter called MBD) did not efficiently express in T98G cells, so we further explored its association with MuvB, using recombinant proteins.

We reconstituted a minimal human MuvB complex in vitro by coexpressing five proteins in Sf9 cells (25). This recombinant MuvB forms a stable complex with full-length recombinant B-Myb that coelutes in size-exclusion chromatography (Fig. 2*A*). To identify the critical MuvB domains for B-Myb association, we implemented a quantitative fluorescence polarization (FP) assay, using a rhodamine-labeled synthetic MBD peptide. We found that the minimal MuvB complex binds B-Myb MBD with high affinity (K_d = 1.2 ± 0.1 nM; Fig. 2*B*). LIN52 is necessary for MMB reconstitution (25), but LIN52 alone bound MBD 150-fold weaker than the MuvB complex, suggesting that additional MuvB proteins contribute to MBD association (Fig. 2*B* and *SI Appendix*, Fig. S2). LIN9 is also required for MMB assembly in cells (16, 20, 30). Although we could not express soluble recombinant LIN9 alone, we could purify a subcomplex including conserved regions in LIN9 (residues 349–466, LIN9$^{349–466}$) and the C terminus of LIN52 (residues 52–116, LIN52$^{52–116}$; *SI Appendix*, Fig. S3). This subcomplex binds B-Myb MBD with similar affinity to the entire minimal MuvB (Fig. 2*B* and *SI Appendix*, Fig. S2), suggesting that LIN9 and LIN52 form the binding interface that recruits B-Myb to the MuvB complex.

We assayed whether the A-Myb and c-Myb MBD sequences, which show some conservation with B-Myb (Fig. 1*A* and *SI Appendix*, Fig. S1), could bind the LIN9$^{349–466}$–LIN52$^{52–116}$ subcomplex, using isothermal titration calorimetry (ITC; Fig. 2*C*). The ITC measurement shows tight association of B-Myb MBD, albeit with weaker affinity than in the FP assay. A-Myb MBD associates with LIN9–LIN52, but with 50-fold weaker affinity than B-Myb, and c-Myb MBD did not produce detectable binding (Fig. 2*C*). These results explain the previous observations that MuvB does not coprecipitate A-Myb or c-Myb as strongly as B-Myb from cell extracts (16, 20). The MBD sequence from *Drosophila* (dMyb), which is representative of the single Myb found in invertebrates (Fig. 1*A* and *SI Appendix*, Fig. S1), binds human LIN9–LIN52 with 13-fold weaker affinity than B-Myb (Fig. 2*C*).

Crystal Structure Reveals the MMB Interface. To resolve the molecular details of the MMB complex, we used anomalous diffraction approaches to solve a 2.3-Å crystal structure of B-Myb MBD bound to the LIN9$^{349–466}$–LIN52$^{52–116}$ subcomplex (Fig. 3 and *SI Appendix*, Fig. S4 and Table S1). The LIN9–LIN52 heterodimer forms a three-stranded antiparallel coiled–coil as the core of the structure (Fig. 3*A*). LIN9 contributes two helices (α1 and α2) that run antiparallel and are connected through a short

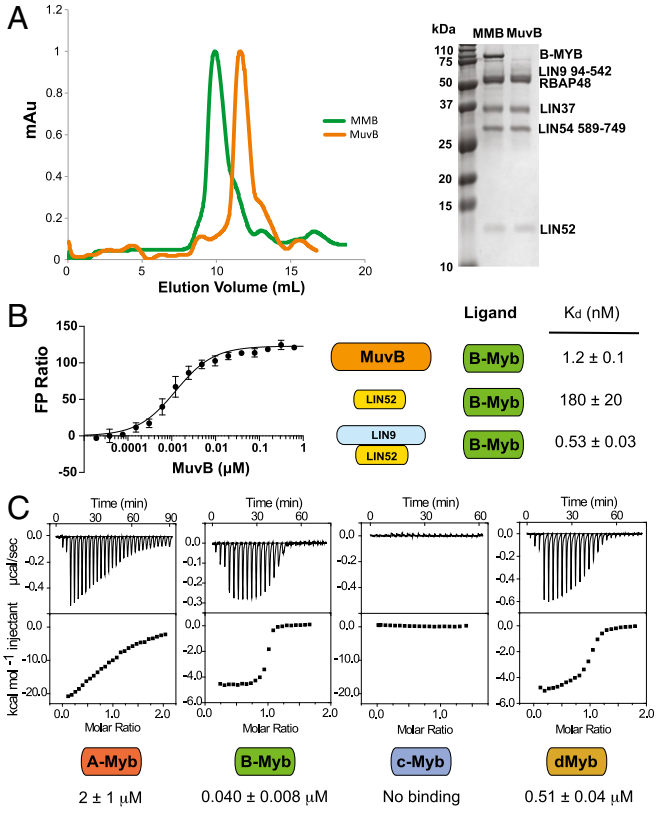

Fig. 2. The Myb MBD directly binds LIN9 and LIN52. (*A*) Superdex 200 chromatograms and a Coomassie-stained SDS/PAGE gel showing proteins in the peak fractions. (*B*) FP measurements of the affinity of the indicted proteins. Data are shown for the labeled MBD peptide titrated with MuvB. (*C*) ITC binding measurements between LIN9$^{349–466}$-LIN52$^{52–116}$ and an MBD peptide from each indicated Myb protein (Fig. 1*A*). Additional raw data for FP and ITC measurements are shown in *SI Appendix*, Fig. S2.

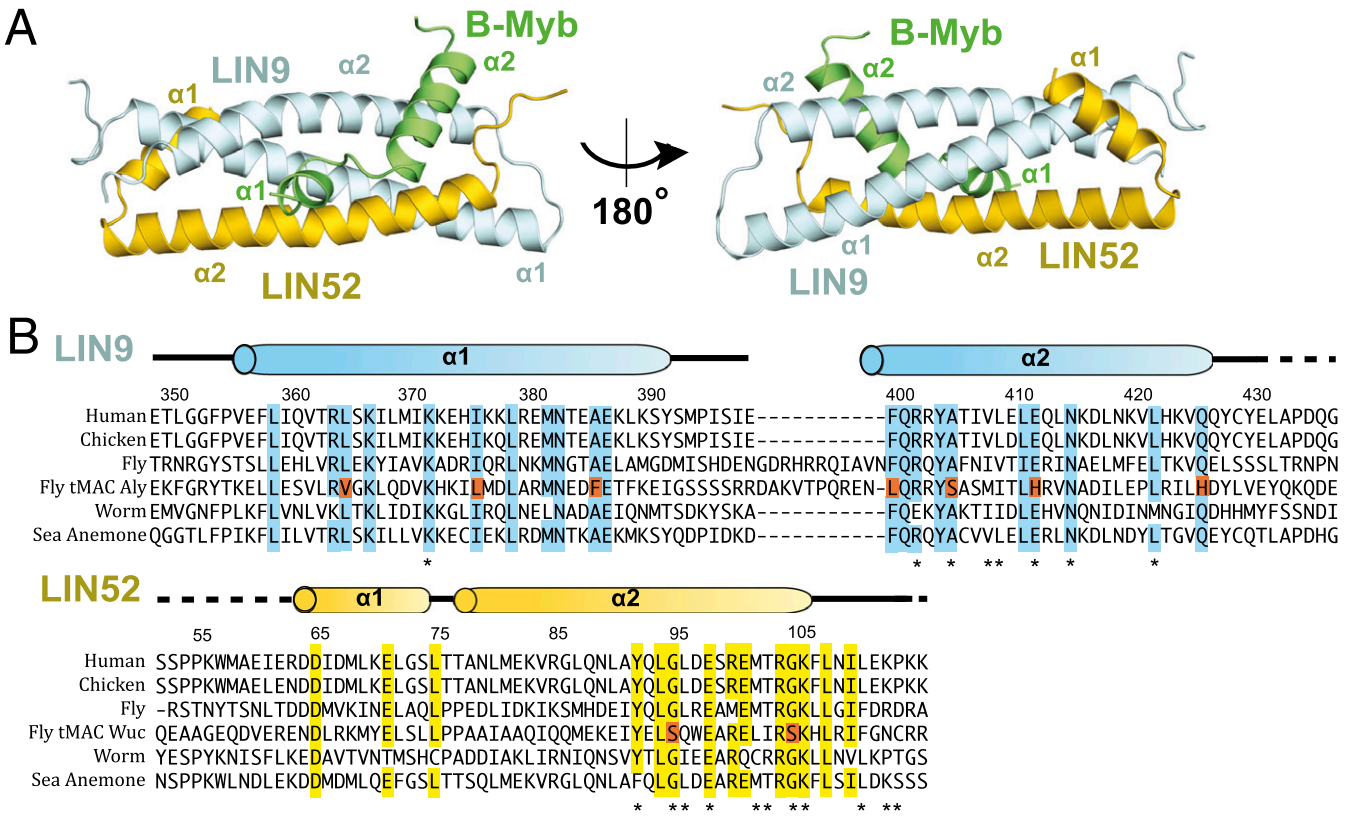

Fig. 3. Crystal structure of the B-Myb MBD bound to the LIN9$^{349–466}$–LIN52$^{52–116}$ heterodimer. (*A*) Overall structure. B-Myb (green) binds the coiled–coil formed by LIN9 (cyan) and LIN52 (yellow). (*B*) Sequence alignments of LIN9 and LIN52 with secondary structure, conservation of primary sequence identity (colored boxes), and MBD-contacting residues (asterisks) indicated. Dashed lines are above sequences that were not included in the model because of a lack of electron density (LIN9 residues 432–466 were also not included). Substitutions in the tMAC paralogs at conserved positions in LIN9 and LIN52 are shaded orange. Sequences are from *Homo sapien*, *Gallus gallus*, *Drosophila melanogaster*, *C. elegans*, and *Nematostella vectensis*.

linker. The third helix is from LIN52 (LIN52 α2) and is parallel with LIN9 α1. LIN52 contains a second shorter helix (α1) that covers a face of the coiled–coil near the N-termini of LIN9 α1 and LIN52 α2.

The B-Myb MBD forms two short helices that bind the coiled–coil surface formed by LIN9 α2 and LIN52 α2 (Fig. 3*A*). The first MBD helix (MBD α1, residues 663–668) is composed of a single turn with its axis pointing toward the center of the coiled–coil. B-Myb residues W663, V666, A667, and C668, which are conserved in many B-Myb orthologs (*SI Appendix*, Fig. S1), make a number of van der Waals contacts with both LIN52 (A91, Y92, L96, and G95) and LIN9 (L418, N419, and L422; Fig. 4*A*). An alanine mutation of LIN52 at Y92, which inserts between B-Myb W663 and V666, reduces affinity of B-Myb 60-fold (Fig. 4*B*). The sidechain of K372 in LIN9 α1, which is conserved in LIN9 orthologs (Fig. 3*B*), forms a hydrogen bond with the backbone carbonyl of A667 in B-Myb. The positive lysine likely stabilizes the negative C-terminal dipole of the MBD α1 helix (Fig. 4*A*), and a LIN9 K372A mutation reduces B-Myb MBD affinity sixfold (Fig. 4*B*). The close approach of MBD α1 to the core of the coiled–coil is possible because of the lack of a sidechain at G95 in LIN52. G95 is conserved in LIN52 (Fig. 3*B*), and a G95S mutation reduces the affinity of the MBD 50-fold (Fig. 4*B*).

The second B-Myb MBD helix (α2) binds the N terminus of LIN9 α2 and the C terminus of LIN52 α2 (Figs. 3*A* and 4*A* and *SI Appendix*, Fig. S5). This interface is primarily stabilized by interactions involving B-Myb residues Q674, M677, A681, and R682 (Fig. 4*A* and *SI Appendix*, Fig. S5). M677 docks into a hydrophobic pocket formed by M102, G105, and K106 in LIN52 and Y404 and V408 in LIN9, whereas A681 contacts L111 in LIN52 and A405, V408, and L409 in LIN9. R682 in MBD α2 makes a salt bridge with E412 in LIN9. We tested substitutions of several of these interacting residues in LIN9 and LIN52, using the FP assay, and in each case found weaker MBD association (Fig. 4*B*). We also found that full-length LIN9 containing a V408A/L409A mutation has weaker affinity for B-Myb, but not LIN37, in a coimmunoprecipitation assay in HeLa cells (Fig. 4*C*). Although we cannot rule out the possibility of additional interactions between the full-length proteins in cells, this coimmunoprecipitation assay result is consistent with the weaker affinity measured using the protein fragments in the FP assay.

Q674 in the B-Myb MBD is also buried at the interface with the LIN9–LIN52 dimer. The glutamine sidechain makes hydrogen bonds with the sidechains of E98 in LIN52 and N415 in LIN9 (Fig. 4*A* and *SI Appendix*, Fig. S5). LIN9 N415 also hydrogen bonds and positions LIN9 K372 for stabilizing MBD α1, whereas LIN52 E98 also hydrogen bonds with the backbone amide of G669 in B-Myb. Together, these four buried polar residues (B-Myb Q674, LIN9 K372, N415, and LIN52 E98) form a hydrogen bond network that brings together all five helices in the coiled–coil and B-Myb (Fig. 4*A*). A LIN52 E98A mutation and LIN9 N415A mutation reduce the MBD affinity 110-fold and 55-fold, respectively, supporting the importance of these interactions (Fig. 4*B*).

Conservation of the MMB Association. The structure of the MBD interface accounts for mutations in dMyb that were deleterious to its function in *Drosophila* (*SI Appendix*, Fig. S6) (14, 15). D673A/Q674A (human B-Myb numbering) and W663A mutants failed to rescue dMyb-deficient cells from arresting in G2/M,

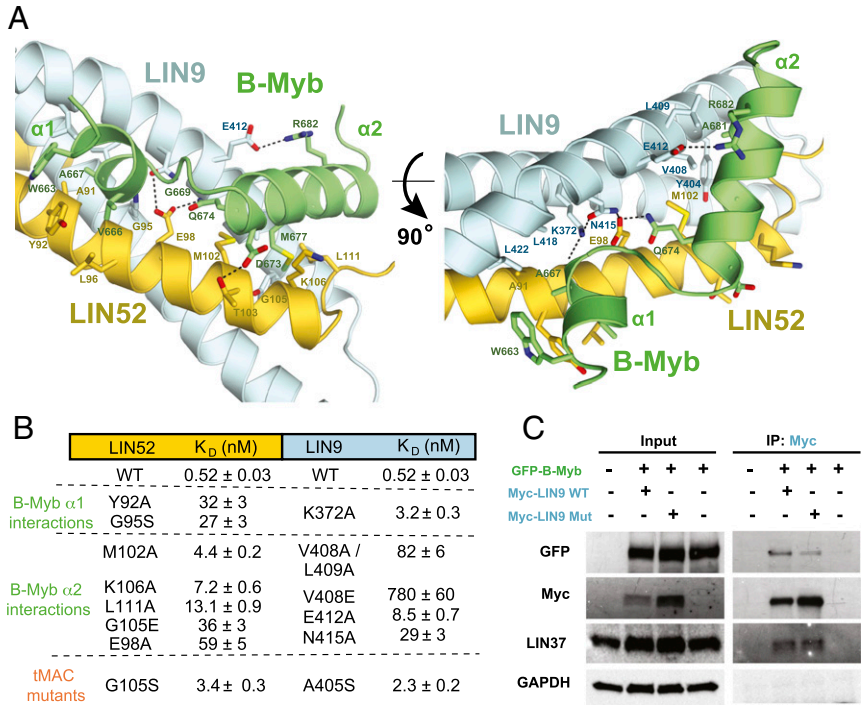

	LIN52	K_D (nM)	LIN9	K_D (nM)
	WT	0.52 ± 0.03	WT	0.52 ± 0.03
B-Myb α1 interactions	Y92A	32 ± 3	K372A	3.2 ± 0.3
	G95S	27 ± 3		
B-Myb α2 interactions	M102A	4.4 ± 0.2	V408A / L409A	82 ± 6
	K106A	7.2 ± 0.6	V408E	780 ± 60
	L111A	13.1 ± 0.9	E412A	8.5 ± 0.7
	G105E	36 ± 3	N415A	29 ± 3
	E98A	59 ± 5		
tMAC mutants	G105S	3.4 ± 0.3	A405S	2.3 ± 0.2

Fig. 4. Interactions stabilizing the MBD interface with LIN9–LIN52. (*A*) View of interface in crystal structure. (*B*) FP measurements of B-Myb MBD binding affinities with $LIN9^{349–466}$–$LIN52^{52–116}$ containing the indicated mutations. Raw data are shown in *SI Appendix*, Fig. S2. (*C*) HeLa cells were transfected with plasmids encoding GFP-B-Myb and Myc-LIN9 fusion proteins, as indicated. LIN9 Mut contains a V408A/L409A mutation. Lysates were immunoprecipitated with an anti-Myc antibody, and Western blots performed to assay the protein of interest. GAPDH is a loading control.

failed to bind to MuvB, and failed to activate expression of a *polo* transgene in vivo (14). Notably, we found that alanine substitutions at M621 or Q618 in dMyb (equivalent to M677 and Q674 in B-Myb) result in loss of association in the ITC assay (*SI Appendix*, Fig. S2). These results, the conservation between B-Myb and dMyb, and the observation that B-Myb can compensate for dMyb in vivo (31) together establish the functional importance of the interface observed in the crystal structure.

The molecular details revealed by the structure of the MBD–LIN9–LIN52 complex also explain the preference of B-Myb over other Myb family members for MuvB (Fig. 2*C*) (20). A large hydrophobic residue is conserved at the M677 position in B-Myb in vertebrates and Myb in simpler metazoans, whereas a serine is substituted in human c-Myb (Fig. 1*A* and *SI Appendix*, Fig. S1). c-Myb, which does not bind LIN9–LIN52 (Fig. 2*C*), also lacks critical interacting residues in the MBD α1 helix (V666 and A667 in B-Myb). A-Myb also contains differences in the MBD α1 helix, which may explain its weaker affinity for MuvB. dMyb does not contain R682 in α1, which makes the salt bridge with LIN9 E412, and it also binds human LIN9–LIN52 with weaker affinity than B-Myb.

The LIN9 and LIN52 residues that are involved in B-Myb binding are conserved among a wide range of metazoans, including *Caenorhabditis elegans*, which does not appear to possess an animal-specific Myb homolog (Fig. 3*B*). The conservation of these regions of LIN9 and LIN52 in *C. elegans* suggests the possibility that this site has an additional function such as recruitment of another protein. The *Drosophila* tMAC complex contains MuvB-like proteins that are specific to the testis (32, 33). The LIN9 paralog Aly (Always early) and the LIN52 paralog Wuc (Wake-up-call) have residue substitutions specifically at regions where B-Myb interacts in our crystal structure (Fig. 3*B*). We found using the FP assay that several of these substitutions (G95S, G105S, and A405S) weaken B-Myb affinity (Fig. 4*B*), consistent with previous observations that tMAC does not bind and functions independently of dMyb (32).

Discussion

We provide here evidence of a direct association among B-Myb, LIN9, and LIN52 via a ternary subcomplex in MMB. The LIN52 protein also mediates assembly of the repressive DREAM complex during quiescence and G1 when phosphorylated at serine 28 by DYRK1A (25, 28). These findings highlight the important role of LIN52 as an adaptor protein that binds either p130 (DREAM) or B-Myb (MMB) to form the proper complex for regulating gene expression at the right time in the cell cycle (Fig. 5). The LIN52 domain that binds B-Myb in our crystal structure does not overlap with the sequence that binds p130. This observation is consistent with our finding that B-Myb and p130 do not directly compete for MuvB association (25) and the observation that dMyb and fly p130 orthologs copurify in the same complex (22). We propose that the interactions between

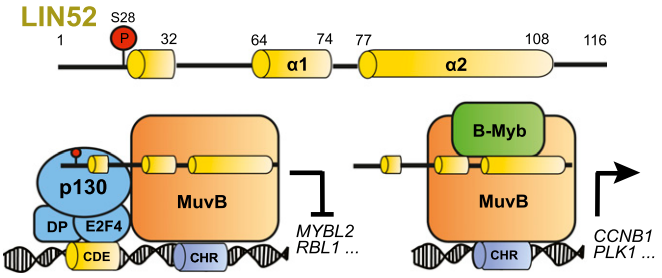

Fig. 5. LIN52 is an adaptor protein that facilitates DREAM and MMB assembly. (*Top*) Domain architecture of LIN52. S28 phosphorylation stimulates association of the LIN52 N terminus with p130. The helices toward the C terminus of LIN52 mediate B-Myb association. LIN52 recruits p130-E2F4-DP to form DREAM during G0/G1 (*Bottom Left*) and B-Myb to form MMB in S/G2 phase (*Bottom Right*), although the interactions are not mutually exclusive. The promoter elements that bind E2F4-DP (CDE) and MuvB (CHR) are shown.

BIOCHEMISTRY

p130 and B-Myb with LIN52 are mutually exclusive in human cells because of the timing of p130 phosphorylation and B-Myb expression. Pocket protein–E2F complexes, including DREAM, have been found to repress the *MYBL2* gene until cell cycle entry (34, 35), and DREAM dissociation through Cdk phosphorylation of p130 occurs as B-Myb levels increase (20, 25).

Previous studies implicate both B-Myb/dMyb and LIN9 as essential for cell-cycle gene activation and progression through mitosis (6, 16–18, 36, 37). Our data suggest that a critical activating function of LIN9 is the recruitment of B-Myb to CHR promoters via the MuvB complex. Similarly, the data suggest that the MBD is essential for B-Myb-mediated gene activation as the site of MuvB association (14, 30). Interestingly, the C terminus of Myb proteins, which includes the MBD, was previously considered to be part of a negative regulatory domain (9–12). The fact that oncogenic C-terminal truncations are exclusive to c-Myb and A-Myb, neither of which bind MuvB strongly, suggests that the C-terminal domain of those paralogs regulates transcription using additional mechanisms that are MuvB-independent. However, it remains possible that these truncations also disrupt binding to the MuvB core that has yet to be detected.

The three *MYB* genes in mammals display distinct phenotypes in knockout studies (6–8), suggesting distinct functions. Phylogenetic analysis indicates that B-Myb is the most ancient vertebrate Myb family member, and only B-Myb can functionally complement the sole Myb in *Drosophila* (31). We found here that dMyb binds LIN9–LIN52 (Fig. 2*C*) with submicromolar affinity, and that many invertebrate Myb proteins contain the critical residues in the B-Myb MBD that contact MuvB. Consistent with these observations, expression of B-Myb but neither c-Myb nor A-Myb can partially rescue a *Drosophila MYB* null mutant (31). Together these results support the idea that the cell-cycle role of B-Myb association with MuvB is among the most conserved functions of Myb, but was lost in the more recently evolved vertebrate paralogs.

The LIN9 and LIN52 helical bundle could serve as a therapeutic target in cancer cells that have high levels of B-Myb expression. In particular, the hydrophobic pocket in which M677 docks appears as a potential site that could bind inhibitors (*SI Appendix*, Fig. S5). Decreased levels of either the MuvB complex protein LIN9 or B-Myb were effective in reducing cancer proliferation and tumor mass (38, 39). Targeting this interface would disrupt the activator MMB complex and potentially restore the DREAM complex to promote quiescence and tumor dormancy (16, 28). The structure of the B-Myb–LIN9–LIN52 interface presented here may benefit future efforts to design cell-cycle inhibitors that target the MMB complex.

Materials and Methods

Protein Expression and Peptides. A glutathione S-transferase (GST) fusion of human LIN52 (residues 52–116) was coexpressed with untagged human LIN9 (349–466) in *Escherichia coli*. Cells were induced with 0.2 mM isopropyl ß-D-1-thiogalactopyranoside and grown overnight at 18 °C. Proteins were first purified with glutathione affinity and anion exchange chromatography. The GST tag was cleaved with TEV protease, and the protein was passed over affinity resin again to remove free GST, and concentrated.

LIN52, LIN37, RBAP48, LIN9 (94–542), LIN54 (589–749), and B-Myb were expressed in Sf9 cells (Expression Systems), using baculoviruses and purified as described earlier (25). Drosophila dMyb (residues 602–632) was expressed in and purified from *E. coli* as a GST fusion protein. The B-Myb$^{657–688}$, SeMet B-Myb$^{657–688}$ and TAMRA-B-Myb$^{657–688}$ peptides were synthesized by Bio-Peptide LLC., and all other peptides were synthesized by GenScript Inc.

Crystallization, Data Collection, Structure Determination, and Model Refinement. The LIN52–LIN9 subcomplex was prepared for crystallization by elution from a Superdex 75 column in a buffer containing 10 mM Tris, 100 mM NaCl, and 1 mM DTT at pH 8.0. B-Myb$^{657–688}$ was added in threefold molar excess to 10 mg/mL LIN52-LIN9. Crystals were grown by sitting-drop vapor diffusion at 22 °C in 100 mM citric acid and 5% PEG 6000 at pH 5. Crystals were frozen in 100 mM Hepes, 10% PEG 400, 20% glycerol, and 1 M NH_4SO_4 at pH 7. Selenomethionine derivative crystals were grown using SeMet B-Myb$^{657–688}$ in 100 mM citric acid and 5% PEG 6000 at pH 5 under Al's oil at 22 °C. Streak seeding using native complex crystals was required for derivative crystal growth.

Data were collected at the Advanced Photon Source, Argonne National Laboratory, at beamline 23-IDB and the Advanced Light Source (ALS), Lawrence Berkeley National Laboratory, at beamline 8.3.1 and 5.0.1. Diffraction spots were integrated using MOSFLM, and data were merged and scaled using Scala. Experimental phasing was solved using Phenix autosol. The model was built with Coot, and the model was refined with Phenix. The complex crystalized with two molecules in the asymmetric unit (*SI Appendix*, Fig. S4). The structural model and structure factors were deposited into the Protein Data Bank under accession code 6C48.

Calorimetry. Isothermal titration calorimetry was performed with a MicroCal VP-ITC system. Peptides and proteins were dialyzed overnight and titrated into a buffer containing 20 mM Tris, 150 mM NaCl, and 1 mM BME at pH 8.0 at 20 °C. To circumvent the difficulty in accurately determining peptide concentration, data fitting was performed by fixing the complex stoichiometry to an equimolar ratio. The molecular stoichiometry observed in the crystal structure supports this assumption in the analysis.

Fluorescence Polarization Assay. TAMRA-labeled B-Myb$^{657–688}$ was mixed at 20 nM with MuvB, LIN52, or LIN9–LIN52 in a buffer containing 50 mM Tris, 150 mM NaCl, 1 mM DTT, 0.1% Tween, at pH 8.0. Twenty microliters of the reaction was used for the measurement in a 384-well plate. FP measurements were made in triplicate, using a Perkin-Elmer EnVision plate reader.

Coimmunoprecipitation Assays. Human T98G cells (#CRL 1690; ATCC) were transiently transfected with pcDNA3.1 vectors encoding a GFP-only control, or GFP-tagged wild-type or mutant B-Myb proteins. HeLa cells (CCL-2; ATCC) were infected with retroviruses produced using pMSCV-Puro vectors encoding HA-tagged wild-type or mutant B-Myb, and selected using 1 μg/mL puromycin. Cell extracts were prepared 36 h later using EBC lysis buffer (50 mM Tris·Cl at pH 7.4, 150 mM NaCl, 0.5% Nonidet P-40, protease and phosphatase inhibitor mixtures) and immunoprecipitated using anti-LIN37 antibody, as previously described (16, 28). Lysates were subjected to Western blot analysis using mouse antibodies to GFP (B-2, sc-9996; Santa Cruz Biotechnology) and p130 (BD Biosciences), as well as rabbit antibodies against LIN9, LIN37, and LIN52 (16, 28). All antibodies were used at 1:1,000 dilution.

ACKNOWLEDGMENTS. This research is supported by NIH fellowship F31CA206244 (to K.Z.G.) and Grants R01CA128836 (to J.S.L.), R01CA188571 (to L.L.), and R01CA132685 and R01GM124148 (to S.M.R.). Data collection on the ALS beamline 8.3.1 is supported by a UC Office of the President, Multicampus Research Programs and Initiatives Grant MR-15-328599.

1. Bandopadhayay P, et al. (2016) MYB-QKI rearrangements in angiocentric glioma drive tumorigenicity through a tripartite mechanism. *Nat Genet* 48:273–282.
2. Ferrarotto R, Heymach JV, Glisson BS (2016) MYB-fusions and other potential actionable targets in adenoid cystic carcinoma. *Curr Opin Oncol* 28:195–200.
3. Ramsay RG, Gonda TJ (2008) MYB function in normal and cancer cells. *Nat Rev Cancer* 8:523–534.
4. Musa J, Aynaud MM, Mirabeau O, Delattre O, Grünewald TG (2017) MYBL2 (B-Myb): A central regulator of cell proliferation, cell survival and differentiation involved in tumorigenesis. *Cell Death Dis* 8:e2895.
5. Sala A (2005) B-MYB, a transcription factor implicated in regulating cell cycle, apoptosis and cancer. *Eur J Cancer* 41:2479–2484.
6. Tanaka Y, Patestos NP, Maekawa T, Ishii S (1999) B-myb is required for inner cell mass formation at an early stage of development. *J Biol Chem* 274:28067–28070.
7. Mucenski ML, et al. (1991) A functional c-myb gene is required for normal murine fetal hepatic hematopoiesis. *Cell* 65:677–689.
8. Toscani A, et al. (1997) Arrest of spermatogenesis and defective breast development in mice lacking A-myb. *Nature* 386:713–717.
9. Sakura H, et al. (1989) Delineation of three functional domains of the transcriptional activator encoded by the c-myb protooncogene. *Proc Natl Acad Sci USA* 86:5758–5762.
10. Dubendorff JW, Whittaker LJ, Eltman JT, Lipsick JS (1992) Carboxy-terminal elements of c-Myb negatively regulate transcriptional activation in cis and in trans. *Genes Dev* 6:2524–2535.
11. Lane S, Farlie P, Watson R (1997) B-Myb function can be markedly enhanced by cyclin A-dependent kinase and protein truncation. *Oncogene* 14:2445–2453.
12. Takahashi T, et al. (1995) Human A-myb gene encodes a transcriptional activator containing the negative regulatory domains. *FEBS Lett* 358:89–96.
13. Oh IH, Reddy EP (1998) The C-terminal domain of B-Myb acts as a positive regulator of transcription and modulates its biological functions. *Mol Cell Biol* 18:499–511.

14. Andrejka L, et al. (2011) Animal-specific C-terminal domain links myeloblastosis oncoprotein (Myb) to an ancient repressor complex. *Proc Natl Acad Sci USA* 108: 17438–17443.
15. Wen H, Andrejka L, Ashton J, Karess R, Lipsick JS (2008) Epigenetic regulation of gene expression by Drosophila Myb and E2F2-RBF via the Myb-MuvB/dREAM complex. *Genes Dev* 22:601–614.
16. Litovchick L, et al. (2007) Evolutionarily conserved multisubunit RBL2/p130 and E2F4 protein complex represses human cell cycle-dependent genes in quiescence. *Mol Cell* 26:539–551.
17. Sadasivam S, Duan S, DeCaprio JA (2012) The MuvB complex sequentially recruits B-Myb and FoxM1 to promote mitotic gene expression. *Genes Dev* 26:474–489.
18. Reichert N, et al. (2010) Lin9, a subunit of the mammalian DREAM complex, is essential for embryonic development, for survival of adult mice, and for tumor suppression. *Mol Cell Biol* 30:2896–2908.
19. Müller GA, et al. (2014) The CHR site: Definition and genome-wide identification of a cell cycle transcriptional element. *Nucleic Acids Res* 42:10331–10350.
20. Pilkinton M, Sandoval R, Colamonici OR (2007) Mammalian Mip/LIN-9 interacts with either the p107, p130/E2F4 repressor complex or B-Myb in a cell cycle-phase-dependent context distinct from the Drosophila dREAM complex. *Oncogene* 26:7535–7543.
21. Beall EL, et al. (2002) Role for a Drosophila Myb-containing protein complex in site-specific DNA replication. *Nature* 420:833–837.
22. Lewis PW, et al. (2004) Identification of a Drosophila Myb-E2F2/RBF transcriptional repressor complex. *Genes Dev* 18:2929–2940.
23. Korenjak M, et al. (2004) Native E2F/RBF complexes contain Myb-interacting proteins and repress transcription of developmentally controlled E2F target genes. *Cell* 119: 181–193.
24. Schmit F, et al. (2007) LINC, a human complex that is related to pRB-containing complexes in invertebrates regulates the expression of G2/M genes. *Cell Cycle* 6: 1903–1913.
25. Guiley KZ, et al. (2015) Structural mechanisms of DREAM complex assembly and regulation. *Genes Dev* 29:961–974.
26. Marceau AH, et al. (2016) Structural basis for LIN54 recognition of CHR elements in cell cycle-regulated promoters. *Nat Commun* 7:12301.
27. Schmit F, Cremer S, Gaubatz S (2009) LIN54 is an essential core subunit of the DREAM/LINC complex that binds to the cdc2 promoter in a sequence-specific manner. *FEBS J* 276:5703–5716.
28. Litovchick L, Florens LA, Swanson SK, Washburn MP, DeCaprio JA (2011) DYRK1A protein kinase promotes quiescence and senescence through DREAM complex assembly. *Genes Dev* 25:801–813.
29. Mages CF, Wintsche A, Bernhart SH, Müller GA (2017) The DREAM complex through its subunit Lin37 cooperates with Rb to initiate quiescence. *eLife* 6:e26876.
30. Osterloh L, et al. (2007) The human synMuv-like protein LIN-9 is required for transcription of G2/M genes and for entry into mitosis. *EMBO J* 26:144–157.
31. Davidson CJ, Tirouvanziam R, Herzenberg LA, Lipsick JS (2005) Functional evolution of the vertebrate Myb gene family: B-Myb, but neither A-Myb nor c-Myb, complements Drosophila Myb in hemocytes. *Genetics* 169:215–229.
32. Beall EL, et al. (2007) Discovery of tMAC: A Drosophila testis-specific meiotic arrest complex paralogous to Myb-Muv B. *Genes Dev* 21:904–919.
33. Doggett K, Jiang J, Aleti G, White-Cooper H (2011) Wake-up-call, a lin-52 paralogue, and always early, a lin-9 homologue physically interact, but have opposing functions in regulating testis-specific gene expression. *Dev Biol* 355:381–393.
34. Lam EW, Watson RJ (1993) An E2F-binding site mediates cell-cycle regulated repression of mouse B-myb transcription. *EMBO J* 12:2705–2713.
35. Liu N, Lucibello FC, Zwicker J, Engeland K, Müller R (1996) Cell cycle-regulated repression of B-myb transcription: Cooperation of an E2F site with a contiguous co-repressor element. *Nucleic Acids Res* 24:2905–2910.
36. Katzen AL, et al. (1998) Drosophila myb is required for the G2/M transition and maintenance of diploidy. *Genes Dev* 12:831–843.
37. Zhu W, Giangrande PH, Nevins JR (2004) E2Fs link the control of G1/S and G2/M transcription. *EMBO J* 23:4615–4626.
38. Iltzsche F, et al. (2017) An important role for Myb-MuvB and its target gene KIF23 in a mouse model of lung adenocarcinoma. *Oncogene* 36:110–121.
39. Wolter P, Hanselmann S, Pattschull G, Schruf E, Gaubatz S (2017) Central spindle proteins and mitotic kinesins are direct transcriptional targets of MuvB, B-MYB and FOXM1 in breast cancer cell lines and are potential targets for therapy. *Oncotarget* 8: 11160–11172.